

Self-organized photosynthetic nanoparticle for cell-free hydrogen production

Ifeyinwa J. Iwuchukwu^{1†}, Michael Vaughn^{2†}, Natalie Myers³, Hugh O'Neill^{2,4}, Paul Frymier^{1,5} and Barry D. Bruce^{1,2,3,5*}

There is considerable interest in making use of solar energy through photosynthesis to create alternative forms of fuel. Here, we show that photosystem I from a thermophilic bacterium and cytochrome-*c*₆ can, in combination with a platinum catalyst, generate a stable supply of hydrogen *in vitro* upon illumination. The self-organized platinization of the photosystem I nanoparticles allows electron transport from sodium ascorbate to photosystem I via cytochrome-*c*₆ and finally to the platinum catalyst, where hydrogen gas is formed. Our system produces hydrogen at temperatures up to 55 °C and is temporally stable for >85 days with no decrease in hydrogen yield when tested intermittently. The maximum yield is ~5.5 μmol H₂ h⁻¹ mg⁻¹ chlorophyll and is estimated to be ~25-fold greater than current biomass-to-fuel strategies. Future work will further improve this yield by increasing the kinetics of electron transfer, extending the spectral response and replacing the platinum catalyst with a renewable hydrogenase.

The world petroleum production rate is predicted to reach its peak before the middle of the century¹ and the higher cost of recovering recalcitrant deposits is expected to drive up the price of petroleum-derived fuels. Although fossil fuels rely on photosynthesis-driven biomass accumulation from millions of years ago, there is hope that directly harnessing photosynthesis can shorten the cycle time for creating fuels from solar energy². Biomass-derived fuels are potentially a clean, renewable and sustainable source of fuel, but several challenges exist. Current biomass-to-fuels schemes yield relatively low fuel value per unit land area; indeed, ethanol produced from switchgrass has a projected gross fuel value yield of 12 litres of gasoline per hectare per day equivalent³. All biomass-to-ethanol technologies produce a dilute mixture of water and ethanol, which needs to be distilled. This accounts for ~20% of the production cost of fuel-grade ethanol³. Furthermore, billions of tons of biomass must be harvested, transported, processed and converted to replace the petroleum used for gasoline in western Europe alone.

One way to improve production yield is to use solar energy directly, as plants do in photosynthesis. Recently, there has been considerable interest in green algae because they can, in principle, use photosynthesis to produce hydrogen from sunlight and water^{4,5}. This hydrogen production is facilitated by specialized pigment–protein complexes known as reaction centres, which span the membranes of plants, algae, cyanobacteria and bacteria^{6,7}. In oxygenic photosynthesis, two reaction centres, photosystem II (refs 8,9) and photosystem I (PSI)^{10–12}, function together in the Z-scheme to transfer electrons derived from water (via photosystem II) to reduce NAD(P)⁺ (via PSI) producing both oxygen and ATP (ref. 13). Coupling either platinum nanoclusters^{14,15} or covalently linked hydrogenase^{16,17} to the acceptor end of PSI complexes can harvest the photochemically produced electrons to reduce protons to hydrogen *in vitro*. Similarly, it has been shown that reaction centres integrated into solid-state devices can be used to produce a photovoltaic current¹⁸.

Here, we show that a stable supply of hydrogen can be generated using a platinum catalyst and a system made of PSI isolated from the thermophilic cyanobacterium *T. elongatus* and a recombinant form of cytochrome-*c*₆ (cyt *c*₆) protein as illustrated in Fig. 1. The thermally stable PSI, which is shown to be more stable than PSI from mesophilic cyanobacteria, shows enhanced hydrogen evolution rates up to 55 °C. Our system can evolve hydrogen for three months without special treatment or chemical preservatives. Under optimized conditions, we estimate that the gross fuel production rate per unit area for these complexes exceeds the best biomass-to-fuel schemes by a factor of 25. We believe that these properties and the renewable nature of PSI and cyt *c*₆ may lead to a sustainable and efficient way to produce alternative fuel.

Isolation of PSI and recombinant cyt *c*₆ from *T. elongatus*

To enable the direct *in vitro* production of hydrogen, we isolated highly purified and highly dispersed PSI particles from both the mesophilic cyanobacterium *Synechocystis* PCC 6803 and the thermophilic cyanobacterium *T. elongatus*. In both PSI preparations, the lowest chlorophyll-containing band of the sucrose gradient typically contained nearly pure trimeric PSI (Fig. 2a). However, the upper band contained significant impurities of the more fluorescent PSII and phycobilisome (PBS) as observed by low-temperature fluorescence (Fig. 2d). Because Tris-tricine sodium dodecyl sulphate polyacrylamide gel electrophoresis (SDS-PAGE; Fig. 2b) revealed the presence of a small amount of PBS proteins, anion exchange chromatography was subsequently used to ensure consistent purity and to concentrate the final preparation of PSI trimers. Transmission electron microscopy (TEM) of the complexes confirmed the uniformity and purity of the trimeric PSI nanoparticles (Fig. 2e). Furthermore, the size distribution of these nanoparticles was investigated by sedimentation velocity (SV) analysis and revealed a single large peak at ~21S (Fig. 2c, blue line). In contrast, the chlorophyll-containing band

¹Department of Chemical and Biomolecular Engineering, University of Tennessee, Knoxville, Tennessee 37996, USA, ²Department of Biochemistry, Cellular and Molecular Biology, University of Tennessee, Knoxville, Tennessee 37996, USA, ³Department of Microbiology, University of Tennessee, Knoxville, Tennessee 37996, USA, ⁴Chemical Sciences Division, Oak Ridge National Laboratory, Oak Ridge, Tennessee 37831, USA, ⁵Sustainable Energy and Education Research Center (SEERC), University of Tennessee, Knoxville, Tennessee 37996, USA; [†]These authors contributed equally to this work.

*e-mail: bbruce@utk.edu

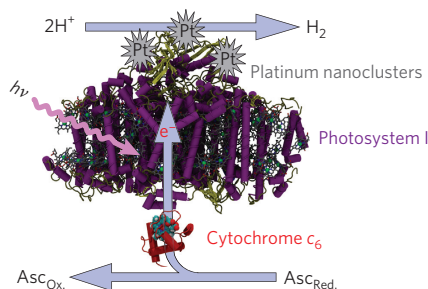


Figure 1 | Schematic of the electron flow in the photosystem I catalytic nanoparticle. The monomeric form of the *T. elongatus* PSI is shown with chlorophyll cofactors (magnesium ligated in macrocycle shown in green van der Waals radius) and the protein coloured by secondary structure (helical regions in purple, beta sheets in yellow and unstructured regions in brown). A partially docked form of the cyt c_6 is shown, providing the re-reduction of P_{700} , deriving electrons from the oxidation of ascorbate ($\text{Asc}_{\text{Red}} \rightarrow \text{Asc}_{\text{Ox}} + e^-$). The platinum clusters on the stromal surface of PSI are shown as grey stars catalysing the reduction of protons to hydrogen with electrons of lower potential via the energy of the absorbed photon, and PSI.

from a PSI sucrose gradient isolation revealed a much smaller monomeric PSI (with a sedimentation coefficient of 12S) and some PSII as indicated by low-temperature fluorescence (Fig. 2d). For reference, we have included a scaled outline of the PSI trimer structure as determined by Jordan and colleagues¹⁹ (Fig. 2e), with the solvent-accessible surfaces of each of the monomers shown in red, blue and purple and their three respective stromal exposed surfaces shown in green. Outlines of these dimensions were drawn in red and placed over several of the nanoparticles observed in the TEM, further confirming the uniformity of our PSI preparation.

To facilitate rapid re-reduction of P_{700} (the special pair of PSI) *in vitro*, it is necessary to have an abundant source of the physiological electron donor cyt c_6 (refs 20,21). The complete *T. elongatus* genome²² revealed only one cyt c_6 gene containing a signal peptide. Using gene-specific primers, the full-length sequence for cyt c_6 was cloned into the pET21b vector and the recombinant protein isolated as described in the Supplementary Information. The correct folding and heme insertion of this recombinant protein were confirmed by the reduced-minus-oxidized difference spectrum (Supplementary Fig. S1) which indicates a β -peak at 552.1 nm, identical to published values for native cyt c_6 isolated from a variety of related cyanobacteria²³.

Thermal stability of purified PSI and cyt c_6

Circular dichroism (CD) spectroscopy was used to measure the thermostability of both PSI and cyt c_6 by monitoring the non-covalent pigment organization of PSI and the protein secondary structure of cyt c_6 . The visible CD spectra of both the mesophilic cyanobacterium *Synechocystis* PCC 6803 and the thermophilic cyanobacterium *T. elongatus* (Supplementary Fig. S2a,b) were similar, as expected for the homologous complexes. The absorbance between 450 and 550 nm is from the bulk antenna chlorophyll associated with PSI, whereas the split exciton signal near 700 nm is derived from the P_{700} special pair²⁴. Figure 3 illustrates the effects of temperature on the arrangement of these pigments. Although both complexes are stable to $\sim 40^\circ\text{C}$, approximately half of the observed absorbance of the bulk chlorophyll is lost by $\sim 55^\circ\text{C}$ for PCC 6803 and $\sim 90^\circ\text{C}$ for *T. elongatus*. Interestingly, the chlorophyll associated with P_{700} maintains its native structure until much higher temperatures for both organisms, maintaining 80% of the maximal absorbance until 70°C and 90°C for *Synechocystis* and *T. elongatus*, respectively. Furthermore, CD experiments indicated cyt c_6 has a T_m of 81°C (Supplementary Fig. S2c).

Rate-limiting step in PSI-mediated hydrogen evolution

Although PSI-mediated photo-production of hydrogen has been demonstrated with PSI isolated from spinach leaves^{14,15} and cyanobacteria¹⁷, this work investigates a similar reaction using thermophilic cyanobacterial PSI. Initial experiments examined the parameters for platinizing *T. elongatus* PSI to support photo-dependent hydrogen evolution. Subsequently, the stability of the system was demonstrated and the effect of each reagent on the rate of hydrogen production was studied.

The role of each component was determined by a sequence-of-addition experiment. The initial reaction containing PSI and $[\text{PtCl}_6]^{2-}$ was allowed to proceed for two light/dark (L/D) cycles, after which the sacrificial electron donor sodium ascorbate was added (marked by a black arrow in Fig. 4a) in the dark, and the rate of hydrogen evolution was continuously monitored at 25°C (Fig. 4a). Very low hydrogen evolution was observed during light cycles before or after ascorbate addition, indicating that ascorbate is inefficient for P_{700}^+ re-reduction. However, addition of cyt c_6 (black arrow with asterisk in Fig. 4a) after six L/D cycles supported a rapid, short-lived burst of H_2 evolution that decreased sharply by the next light cycle. This behaviour indicates rapid reduction of the pool of reduced cyt c_6 as the platinum catalyst deposits on PSI, causing the rate of H_2 evolution to drop. The system is in equilibrium when the rate of cyt c_6 reduction by ascorbate matches the level of P_{700} photo-oxidation, causing H_2 evolution to become constant with each light cycle.

The platinum catalyst was shown to be tightly associated with PSI nanoparticles using energy-dispersive X-ray spectroscopy of previously platinized PSI nanoparticles that had been re-isolated and dialysed overnight. As shown in Fig. 4b, this sample clearly contains platinum, as indicated by the energy levels of the emitted X-rays with characteristic energies (2.05, 11.07/11.25 and 9.36/9.44 keV). Finally, the catalytic activity of the previously platinized PSI was confirmed to not require additional platinum (Fig. 4c). Limited hydrogen evolution was observed before the addition of ascorbate and cyt c_6 . The lack of hydrogen evolution detected on addition of ascorbate indicates that the re-isolated PSI did not contain cyt c_6 . Moreover, addition of fresh cyt c_6 increased the rate of hydrogen evolution by a factor of ~ 80 . These experiments indicate that the initial platinization results in platinum integration into PSI that is both stably associated and catalytically active. Although the exact molecular-level structure of this platinization is not known, electron microscopy analysis indicates that the platinum forms electron-dense complexes associated with PSI (Supplementary Fig. S3) Following this burst in hydrogen evolution, we observe a slow decay in hydrogen evolution that can be fit to a single exponential decrease with a half-life of 3.8 h (shown in Fig. 4c).

The light saturation experiment was performed with platinized *T. elongatus* PSI nanoparticles similar to those described above. The hydrogen production rate increased with increasing light intensity (Fig. 4d) and began to plateau as the light intensity approached $800 \mu\text{E m}^{-2} \text{s}^{-1}$; however, this curve is sigmoidal with a distinct lag phase. Although these data cannot be well fit to a simple single-substrate kinetic model (dashed line), it can be fit to a cooperative model (solid line) with a Hill coefficient of ~ 2.5 . The shape of this curve is different from the light saturation response for monomeric PSI isolated from spinach¹⁵, which was linear in the low light region. Because the *T. elongatus* PSI (Fig. 2e) is trimeric, the platinum catalyst can potentially accept electrons from more than one of the PSI P_{700} in the trimeric complex. Such cooperativity between adjacent PSI monomers explains how a single electron from a single P_{700} could facilitate molecular hydrogen production, which requires two electrons to reduce two protons. This sigmoidal response indicates that at higher light levels the probability of simultaneously photo-exciting two PSI reaction centres increases within a trimer, thus yielding a higher and 'cooperative' mechanism of

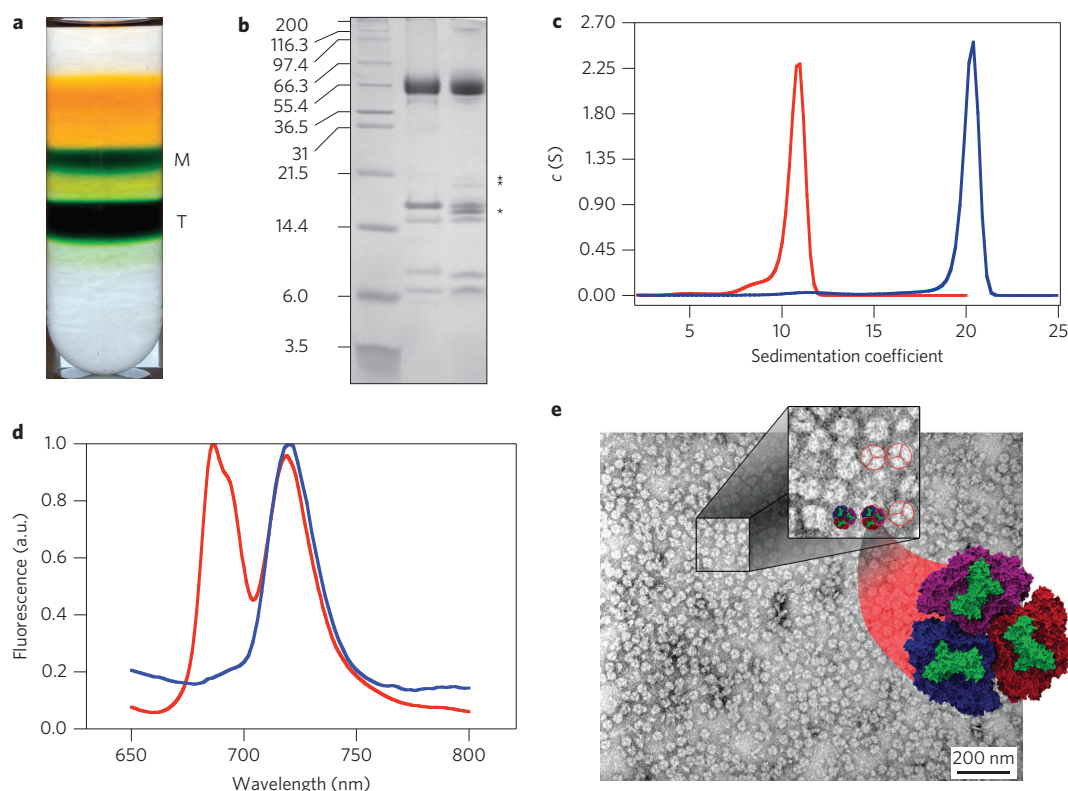


Figure 2 | Isolation of photosystem I. **a**, Typical 10–30% sucrose density gradient displaying complete resolution of trimeric PSI (**T**) from monomer and PSII (**M**). **b**, Tris-tricine SDS-PAGE of PSI preparations from *T. elongatus* (lane 2) and *Synechocystis* PCC 6803 (lane 3); phycobiliproteins are indicated by asterisks and the other bands are subunits of PSI. **c**, Sedimentation velocity analysis of monomer and trimer fractions was analyzed using a sedimentation coefficient distribution analysis, $c(s)$. The Y-axis values are on a relative scale. Trimeric PSI appears as a single peak (blue) with a sedimentation coefficient of 21S, whereas the monomer has peak values of approximately 12S and 8S (red). **d**, Low-temperature fluorescence indicates a highly fluorescent component emitting below 700 nm (red line) within the upper band, likely PSII and/or allophycocyanin, but a single emission maximum at 730 nm (blue line) as expected for intact PSI trimers. **e**, TEM image of purified trimeric PSI. Inset: magnified $\times 2.5$ and directly compared with a scaled space-filling model of PSI. Transmembrane elements of each monomer are shown as red, blue or purple, and stromal external subunits are green.

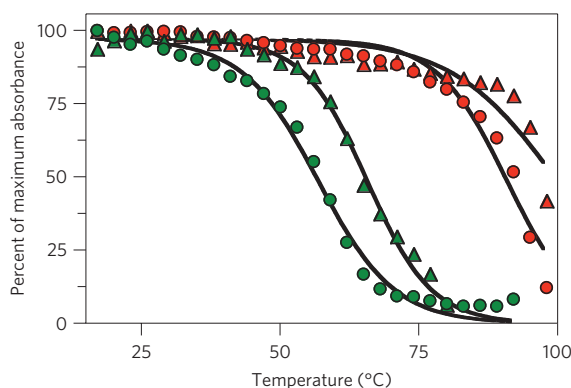


Figure 3 | Thermal stability of photosystem I monitored by circular dichroism. The normalized maximal absorbance for each of the datasets shown in Supplementary Fig. S2a,b are shown as a function of temperature; green symbols indicate data for *Synechocystis* PCC 6803 and the red symbols indicate *T. elongatus*. In both cases, circles indicate antenna chlorophyll (positive peak at 515 nm) and the triangles indicate the split exciton signal originating from P_{700} (minima at 700 nm).

hydrogen production. Another difference between the spinach and *T. elongatus* light responses was the light level at which the hydrogen yield was observed to plateau. In spinach, the plateau was at $\sim 200 \mu\text{E m}^{-2} \text{s}^{-1}$, whereas in *T. elongatus* the plateau was at $\sim 800 \mu\text{E m}^{-2} \text{s}^{-1}$. This may be the result of the considerable

difference in the chlorophyll antennae-to- P_{700} ratio in the organisms. The plant PSI has much larger antennae, approaching ~ 300 chlorophyll/ P_{700} whereas the *T. elongatus* PSI is ~ 95 chlorophyll/ P_{700} . This approximately threefold difference in antenna size would account for the difference in light dependence.

Evaluation of hydrogen production

To evaluate the temporal stability of this cell-free hydrogen evolution system, we tested one preparation of platinumized PSI repeatedly over three months. The temporal details of this experiment are described in the Supplementary Information. These data show that our PSI preparations maintain operational stability for extended time periods. Representative data from three L/D cycles throughout this 85-day experiment are shown in Fig. 5a. By directly comparing the hydrogen yield observed initially with that observed after 85 days, it is clear that the yields are identical, as shown in Fig. 5b. This indicates that without special precautions or additives, the platinumized *T. elongatus* PSI complex is capable of constant hydrogen evolution for more than 85 days of intermittent testing and storage.

To optimize hydrogen evolution from this thermophilic PSI system, we examined the effect of temperature on hydrogen evolution rates *in vitro*. We have already determined that $\text{cyt } c_6$ and PSI have T_m values of 81°C and $\sim 90^\circ\text{C}$, respectively (Fig. 3 and Supplementary Fig. S2c) and observed an 80% increase in hydrogen yield when the temperature was raised to 60°C (Fig. 5a). We therefore repeated this temperature dependence measurement using a fresh platinumized PSI preparation (Fig. 5c). The yield of integrated hydrogen evolution increased between 25°C and 55°C , as shown

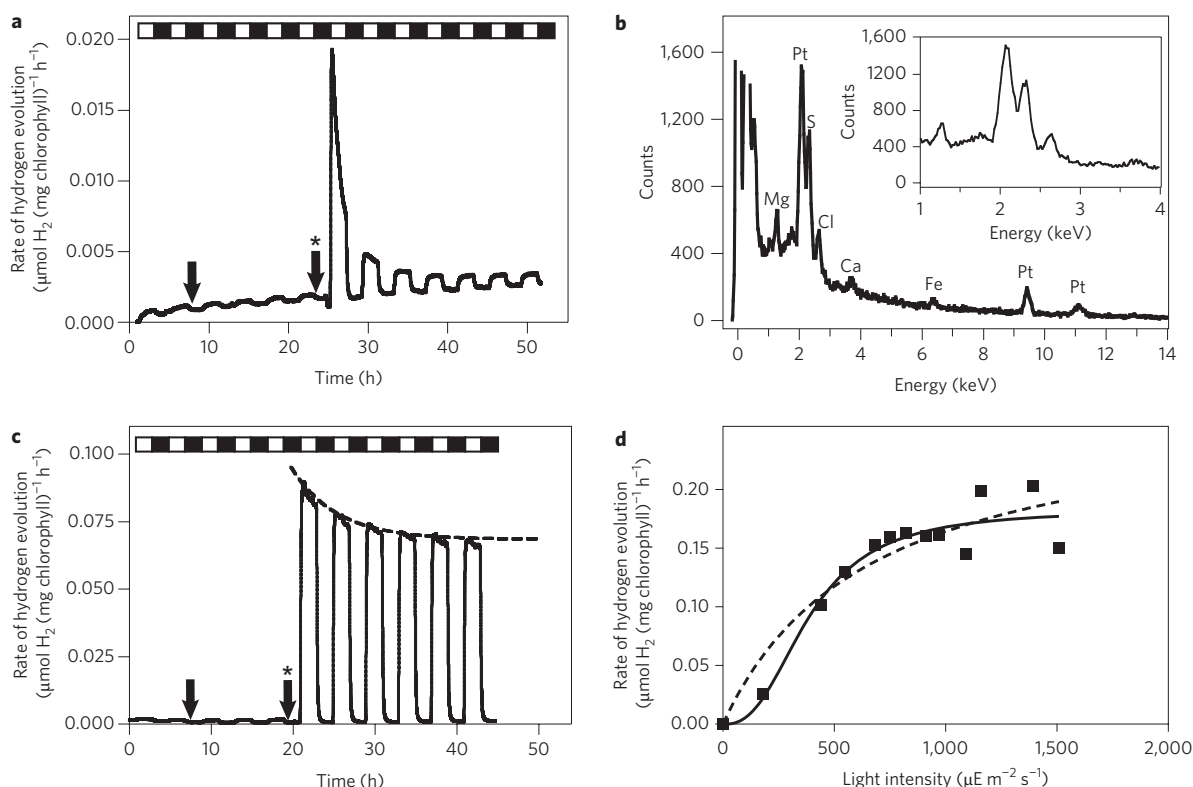


Figure 4 | Determining the role of each component in PSI-mediated hydrogen evolution. **a**, PSI and PtCl_6^{2-} proceeded at 25°C for two light/dark cycles before addition of 1 mM NaAsc at $t = 7$ h (first arrow) and cyt c_6 at $t = 25$ h (second arrow with *). **b**, Energy-dispersive X-ray spectroscopy confirms platinum nanoclusters. The inset indicates the primary platinum transition, M_{α_1} , at 2.05 keV. **c**, Beginning with PtCl_6^{2-} and cyt c_6 -free platinized PSI, 1 mM NaAsc was added at $t = 7.5$ h (first arrow), with no significant hydrogen production. At $t = 20$ h, cyt c_6 was added (second arrow with asterisk), leading to the onset of hydrogen production with the next light cycle, indicating the necessity of cyt c_6 , PSI and NaAsc, and the stability of the preformed platinum nanoclusters because no additional platinum salts are required. **d**, Previously platinized PSI ($20 \mu\text{g chlorophyll ml}^{-1}$) was used to determine hydrogen production as a function of light intensity. The data were fit to a single site kinetic model, that is, with no cooperativity (dashed lines), and a cooperative model (solid line). Checkered bars in **a** and **c** indicate dark/light cycles.

in Fig. 5c. Further increase in the temperature above 55°C (the physiological growth temperature) resulted in a slow decrease in the rate of hydrogen evolution. A slight decrease in the hydrogen evolution rate as a function of temperature was observed (Fig. 5c) above 55°C (ref. 25). However, a similar decrease in the rate of hydrogen evolution with subsequent L/D cycles where the temperature was fixed at 25°C was observed (Fig. 4c). Fitting both of these observed decreases in hydrogen evolution (Figs 4c and 5c) yielded a single exponential decay with a similar half-life of 3.76 h. This similarity in kinetics suggests some system component is slowly losing its activity during multiple L/D cycles.

Being the only consumable component, it is possible that ascorbate is degraded or consumed to sub-saturating levels during longer experiments. To test the limiting role of ascorbate, we ran a 70-h experiment as shown in Fig. 5d. We observed a decrease in yield best fit by the sum of two exponentials (half-lives 19.8 h and 4.64 h). The faster decay is similar to that observed in Figs 4c and 5c. At ~ 70 h, fresh ascorbate was injected (black arrow, Fig. 5d) yielding an immediate $\sim 80\%$ increase in H_2 evolution, with no decay evident for the next 30 h. This experiment shows that part of the decrease in yield is due to ascorbate consumption, which is reflected in this slow phase. The initial loss of activity is possibly a result of catalyst poisoning. Platinum and other platinum group metal catalysts are sensitive to poisoning by a wide range of compounds including sulphur-containing compounds²⁶, heterocyclic nitrogen-containing compounds²⁷ and other surface adsorbing molecules. Chlorophyll, a five-membered heterocycle, is a known poison for some metal-based catalysts²⁸. It is possible that either free chlorophyll or some other degradation product is

responsible for this decrease in activity. A second explanation is that chlorophyll could be lost from PSI over time, leading to a direct decrease in the antenna size and rate of photon capture. During extended periods (>24 h) there is a measurable loss of chlorophyll from the PSI complex as determined by absorption spectrometry (Supplementary Fig. S4). This chlorophyll release could account for the initial change in hydrogen evolution rate over time, either by its poisoning of the platinum catalyst or by simply reducing the amount of chlorophyll in PSI or some combination of these processes. However, in long-term experiments (Fig. 5a) the rate becomes constant, indicating that the system is stable for months of operation after an early initial decrease in activity.

To compare the temperature dependence of hydrogen production for PSI from *T. elongatus* and *Synechocystis* PCC 6803, the integrated yield of hydrogen for a 2-h light cycle was measured and plotted against temperature. It is clear that for *T. elongatus* the hydrogen yield increased up to 55°C before it began to decrease (Fig. 5c,e); however, the hydrogen yield for *Synechocystis* PCC 6803 decreased steadily and was barely detectable at 60°C . The experiments above illustrate the thermal ($>55^\circ\text{C}$) and temporal ($>2,000$ h) stability achievable with these hydrogen-evolving nanoparticles. The hydrogen evolution rates shown in Fig. 4c ($\sim 80 \text{ nmol H}_2 \text{ h}^{-1} (\text{mg chlorophyll})^{-1}$) equal or exceed those previously reported using platinized PSI from plants^{14,15}.

In the final experiment, reaction conditions were altered to allow comparison to a recent publication²⁹ and are described in the Methods. Under these conditions, a maximum rate of $>5.5 \mu\text{mol H}_2 \text{ h}^{-1} (\text{mg chlorophyll})^{-1}$ was obtained (Fig. 6). Our maximum

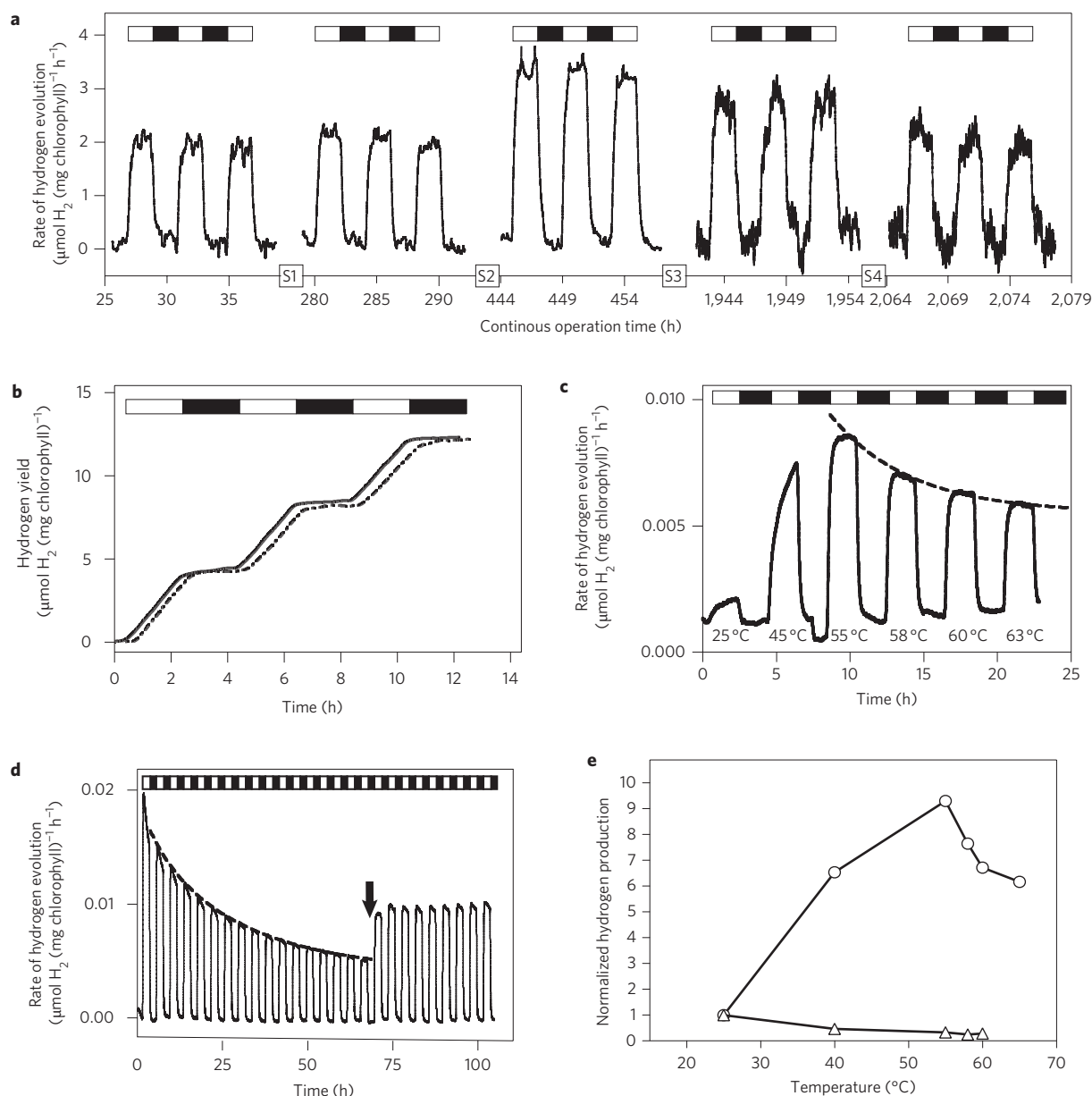


Figure 5 | Thermal and temporal stability of hydrogen evolution. **a**, A single sample was repeatedly measured for ~ 86 days. Selected data are shown: three light/dark (L/D) cycles following 60 h platinization; exhaustive dialysis to remove platinite (S1); followed by 170 h at 25 °C (three L/D cycles shown and remaining as S2); three L/D cycles at 60 °C; stored for 64 days at 4 °C (S3); sample was re-tested for three L/D cycles at 25 °C; stored for 5 days (S4); finally tested for three L/D cycles. **b**, Integrated hydrogen yield of three L/D cycles shown at the beginning before S2 (solid line) and at the end after S4 (dashed line), both at room temperature, 25 °C. **c**, Temperature-activity measurements of *T. elongatus* PSI. **d**, Ascorbate consumption. Addition of 1 mM ascorbate at $t = 68$ h (arrow) increased yield, suggesting the initial 2 mM ascorbate has become limiting after the first 17 L/D cycles. The decrease in activity is fit by a single exponential in panels **c** and **d**. **e**, Comparison of hydrogen yield of *T. elongatus* (open circles) and *Synechocystis* (open triangles) PSI with increasing temperature. Integrated hydrogen yield over 2 h light cycles are normalized by dividing by their respective 25 °C yields.

rate is of the same magnitude as that recently reported for a tethered PSI nanoparticle complex used by Grimme and colleagues²⁹. In that study, pre-formed platinum/gold nanoparticles coupled directly to cyanobacterial PSI were used to evolve hydrogen. They reported a rate of $\sim 45 \mu\text{mol H}_2 \text{ h}^{-1} (\text{mg chlorophyll})^{-1}$. Unlike the self-organizing *in situ* platinization procedure used in the current study, this group rebuilt the native PSI to incorporate a recombinant form of the PsaC subunit containing a free cysteine that allowed the covalent attachment of preformed platinum-gold nanoparticles. The peak rate for our system is also an order of magnitude higher than the hydrogen evolution rates of $\sim 580 \text{ nmol H}_2 \text{ h}^{-1} (\text{mg chlorophyll})^{-1}$ that have

been reported using a [NiFe]-hydrogenase from *Ralstonia eutropha* fused directly to PsaE of PSI from *Synechocystis* PCC 6803 (ref. 17). An additional advantage of the *in situ* approach is that it requires at least a 50-fold lower level of platinum salts ($70 \mu\text{M}$ versus $3.4 \text{ mM H}_2\text{PtCl}_6$) than the rebuilt tethered system. This is an important difference in light of the potential sustainability of such a hydrogen source. The platinized system can maintain a high level of hydrogen production over long periods ($>2,000$ h), whereas the hydrogenase system described above becomes inactive in less than 200 min and the stability of the system of Grimme and colleagues using a rebuilt PSI complex has not been tested beyond 12–16 h.

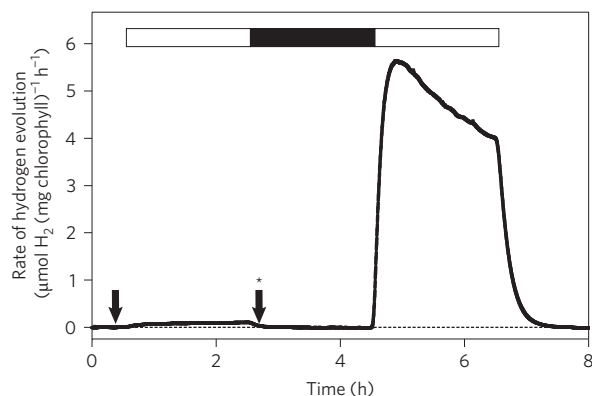


Figure 6 | Peak rates of hydrogen evolution. Platinized PSI complexes ($5 \mu\text{g}$ chlorophyll ml^{-1}) were illuminated in the presence of 100 mM ascorbate (first arrow) and 20 mM MES buffer pH 6.4. White light from a halogen bulb light source was used at an intensity of $1,200 \mu\text{E m}^{-2} \text{ s}^{-1}$. Cyt c_6 was added at a final concentration of $4.4 \mu\text{M}$ into the system at time $t = 2.8 \text{ h}$, in the dark, as indicated with the second arrow with asterisk.

Discussion

In summary, we have demonstrated a simple ‘rewiring’ of the electron transport pathway of PSI that permits a productive interface with a self-organized platinum catalyst (Fig. 1). This light-driven catalytic production of hydrogen is both temporally and thermally stable. Simple optimization of this self-organized system leads to rates close to those recently reported by researchers working with synthetically attached catalysts. Additionally, we showed that increasing the temperature to 55°C increases our rates by a factor of ~ 15 (Fig. 5c), which considerably exceed the rates of other available methods while retaining the benefit of a self-organizing system. If scaled linearly, a solar collector 1 acre in size with a solution depth of 10 cm operating at 55°C would be capable of producing hydrogen with an energy yield equivalent to that of 300 litres of gasoline per hectare per day (gross yield, ignoring production separation and distribution energy costs; see Supplementary data). This potential yield is more than an order of magnitude higher than the gross yield in terms of gasoline equivalents of agricultural biomass systems such as corn-based ethanol (5.43 litres per day per hectare), soy based biodiesel (1.42 litres per day per hectare) or projected yields of switchgrass-produced ethanol (12.1 litres per day per hectare). Comparing this fuel production rate to the average available solar radiation at latitudes in the middle of the US, this system is capable of converting $\sim 6\%$ of solar radiation into usable fuel. This system provides a more direct route to fuel production with no need for the harvesting, converting, fermenting and distilling processes involved in conversion of biomass to ethanol. Moreover, other processing and transportation costs would be much lower because the bio-platinum hybrid catalyst is reused through many cycles, unlike in single-use methods such as biomass accumulation. Finally, the fact that our PSI operates with high thermal tolerance suggests that this approach may be viable in non-arable regions with high solar irradiances. This is in contrast to the cultivation of biofuels that may compete directly with agricultural production.

Methods

Growth of *T. elongatus*. The thermophilic cyanobacterium *T. elongatus* BP-1 was grown in 2-l airlift fermenters (Bethesda Research Labs) in nitrilotriacetic acid (NTA) media. The temperature was held at 55°C with continuous illumination by fluorescent lights. The light level was increased as the cultures approached higher densities to a maximum of $50 \mu\text{E m}^{-2} \text{ s}^{-1}$. Cells were collected during late log phase by centrifugation for 10 min at $7,000g$, and washed once in wash buffer (20 mM 2-(*N*-morpholino)ethanesulphonic acid (MES) pH 6.5, 5 mM MgCl_2 and 5 mM CaCl_2) before storage at -20°C until use for PSI preparation.

Isolation of PSI. Frozen cells were resuspended in wash buffer and 500 mM sorbitol. The resuspended cells were adjusted to a chlorophyll *a* content of 1 mg ml^{-1} and homogenized using a Dounce homogenizer. Lysozyme was added to 0.2% (w/v) and the mixture was incubated for 2 h at 37°C with shaking. The resulting mixture was centrifuged for 10 min at $7,000g$ and the light blue supernatant was discarded. The pellet was resuspended in the wash buffer. The volume was adjusted again so that the chlorophyll *a* concentration was 1 mg ml^{-1} ; the mixture was then passed twice through French Press (Amino) at a cell pressure of $20,000 \text{ psi}$. The highly fluorescent lysate was centrifuged at $\sim 50,000g$ for 20 min, and the supernatant was discarded. The crude membrane fragments collected in the pellet were washed in wash buffer supplemented with 3 M NaBr and then twice in the initial wash buffer. The final washed membrane fragments were adjusted to a chlorophyll *a* concentration of 1 mg ml^{-1} and dodecyl-maltoside (DM) was added to a final concentration of 0.6% w/v and the mixture incubated for 20 min at 20°C in darkness with gentle stirring. The insoluble material was removed from the solubilized membrane mixture by centrifugation at $50,000g$ for 30 min. The supernatant was separated immediately from the pellet and then loaded onto $10\text{--}30\%$ sucrose gradients with 60% cushion; all solutions in the gradient also contained 20 mM MES pH 6.5 and 0.03% DM. Density gradient centrifugation was performed at $\sim 80,000g$ at 10°C for 16 h. The lowest green band contained the trimeric PSI complex; these bands were collected and pooled using a large syringe. Pooled PSI samples were slowly diluted fivefold by addition of 20 mM MES pH 6.5 with 0.03% DM (w/v), and then loaded onto a POROS 20HQ (Applied Biosystems) anion exchange column and eluted with a linear 0 to 400 mM MgSO_4 gradient. The MgSO_4 was removed by dialysing against 20 mM MES pH 6.5, $500 \mu\text{M}$ CaCl_2 , $500 \mu\text{M}$ MgCl_2 and 0.03% DM, and aliquots were stored at -80°C for future use.

CD, secondary structure deconvolution and thermal stability of PSI and cyt c_6 . CD of purified PSI was measured in the visible region from 350 to 750 nm using an Aviv 202 (AVIV Biomedical). Spectra were collected across a temperature range of $15\text{--}95^\circ\text{C}$ in increments of 3° ; at each temperature the sample was equilibrated for 3 min before collecting the data with a step size of 1 nm and integration of 1 s . Similarly, the cyt c_6 was scanned between 15 and 95°C in 5°C increments.

Real-time hydrogen detection and calibration. An in-house developed continuous flow system was used for hydrogen detection. A humidified nitrogen stream flowing at 50 ml min^{-1} carried the hydrogen produced in the reaction chamber to an in-line Figaro tin oxide hydrogen sensor (model TGS821, Figaro Engineering). The signal from the hydrogen sensor was transmitted to a Keithley model 2000 auto-ranging digital multimeter via a bridge amplifier as described previously¹⁵. The sample was illuminated by means of a dual Fiber-Lite A3200 fibre-optic illuminator with an OSRAM 150 W quartz halogen lamp (Dolan-Jenner Industries). Light was filtered through a 590-nm long-pass filter and measured with a Licor quantum flux meter (Model Li-189). For the light saturation and temperature dependence experiments, a Fisher Scientific fibre-optic illuminator (Model 12-562-36) fitted with dual fibre-optic cables was used, and an USHIO 150 W halogen projector lamp (USHIO INC) calibrated using the LI-1800 portable spectroradiometer (LI-COR). At each power setting on the fibre-optic illuminator, the micro-processor-controlled LI-1800 spectroradiometer was used for rapid acquisition of spectroradiometric and photometric data.

PSI-mediated hydrogen evolution. Platinization reactions were carried out by incubation of cyt c_6 , PSI (*T. elongatus* or *Synechocystis*) and 0.5 mM $\text{Na}_2[\text{PtCl}_6]$ in a thermostatically controlled photo-bioreactor as described previously¹⁵, except that 20 mM MES at pH 6.4 was used to buffer the reaction. The molar ratio of cyt c_6 to *T. elongatus* PSI was maintained at 10:1, unless otherwise stated. Typical reactions contained PSI ($80 \mu\text{g}$ chlorophyll ml^{-1}), $282 \mu\text{mol}$ cyt c_6 , 0.5 mM $\text{Na}_2[\text{PtCl}_6]$, 20 mM MES buffer pH 6.4 and 20 mM (1 mM in some cases) NaAsc, at 25°C . All reaction components, except NaAsc, were combined and injected into the photo-bioreactor. After anaerobiosis was achieved ($\sim 1 \text{ h}$) the NaAsc was added to the reaction. Samples were illuminated as described above. A Chronrol Model XT microprocessor-based timer was used to cycle the light on and off at intervals of 2 h. The photo-bioreactor was shielded from external light. After 24 h of the light-catalysed platinization and hydrogen evolution, the reaction mixture was dialysed in 20 mM MES buffer pH 6.4, to remove excess hexachloroplatinate. In some cases, sucrose density gradient centrifugation was used to remove small analytes but had the additional effect of separation of the PSI complexes and cyt c_6 .

Temperature-activity measurements were carried out as described above using the dialysed platinized PSI preparation. The reactions were carried out in 20 mM MES pH 6.4 with 20 mM NaAsc as the sacrificial electron donor. No additional cyt c_6 or $\text{Na}_2[\text{PtCl}_6]$ were added to these reactions. An external water bath was used to incrementally increase the temperature during successive 2 h light on/off cycles, allowing the reaction to equilibrate during the dark cycles. A thermocouple was inserted into the reaction mixture to directly measure the temperature of the reaction. For long-term stability, hydrogen evolution was measured as above, and the data were integrated as a function of time with a smoothing window of 13 data points (Fig. 4b), demonstrating the compatible yield upon long-term storage.

For the peak yield experiment in Fig. 5, the PSI complexes were platinized as described above, except that the chlorophyll and hexachloroplatinate concentrations were reduced to $5 \mu\text{g ml}^{-1}$ and $70 \mu\text{M}$, respectively. After ten light cycles, the PSI

complexes were recovered and purified by density gradient centrifugation. The purified PSI complexes were resuspended in reaction media at a cyt c_6 to P₇₀₀ molar ratio of 75, with an illumination level of $\sim 1,200 \mu\text{E m}^{-2} \text{s}^{-1}$, a NaAsc concentration of 100 mM and a temperature of 25 °C.

Received 16 June 2009; accepted 26 September 2009;
published online 8 November 2009

References

1. Tsoskounogiou, M., Ayerides, G. & Tritopoulou, E. The end of cheap oil: current status and prospects. *Energy Policy* **36**, 3797–3806 (2008).
2. Moore, A. Short-circuiting our fossil fuel habits. Could a more direct harnessing of photosynthesis become an alternative to natural oil, coal and gas? *EMBO Rep* **6**, 205–208 (2005).
3. Pimentel, D. & Patzek, T. Ethanol production using corn, switchgrass and wood; biodiesel production using soybean and sunflower. *Natural Resources Res.* **14**, 65–76 (2005).
4. Ghirardi, M. L. *et al.* Microalgae: a green source of renewable H₂. *Trends Biotechnol.* **8**, 506–511 (2000).
5. Ghirardi, M. L. *et al.* Hydrogenases and hydrogen photoproduction in oxygenic photosynthetic organisms. *Ann. Rev. Plant Biol.* **58**, 71–91 (2007).
6. Deisenhofer, J. & Michel, H. High-resolution structures of photosynthetic reaction centers. *Ann. Rev. Biophys. Biophys. Chem.* **20**, 247–266 (1991).
7. Golbeck, J. H. Shared thematic elements in photochemical reaction centers. *Proc. Natl Acad. Sci. USA* **90**, 1642–1646 (1993).
8. Iwata, S. & Barber, J. Structure of photosystem II and molecular architecture of the oxygen-evolving centre. *Curr. Opin. Struct. Biol.* **14**, 447–453 (2004).
9. Kalman, L., Williams, J. C. & Allen, J. P. Comparison of bacterial reaction centers and photosystem II. *Photosynth. Res.* **98**, 643–655 (2008).
10. Grotjohann, I. & Fromme, P. Structure of cyanobacterial photosystem I. *Photosynth. Res.* **85**, 51–72 (2005).
11. Nelson, N. & Ben-Shem, A. The structure of photosystem I and evolution of photosynthesis. *Bioessays* **27**, 914–922 (2005).
12. Jensen, P. E. *et al.* Structure, function and regulation of plant photosystem I. *Biochim Biophys. Acta* **1767**, 335–352 (2007).
13. Barber, J. Photosystem II: the engine of life. *Q. Rev. Biophys.* **36**, 71–89 (2003).
14. Evans, B. R. *et al.* Enhanced photocatalytic hydrogen evolution by covalent attachment of plastocyanin to photosystem I. *Nano Lett.* **4**, 1815–1819 (2004).
15. Millsaps, J. F., Bruce, B. D., Lee, J. W. & Greenbaum, E. Nanoscale photosynthesis: photocatalytic production of hydrogen by platinumized photosystem I reaction centers. *Photochem. Photobiol.* **73**, 630–635 (2001).
16. Ihara, M. *et al.* Photoinduced hydrogen production by direct electron transfer from photosystem I cross-linked with cytochrome c(3) to [NiFe]-hydrogenase. *Photochem. Photobiol.* **82**, 1677–1685 (2006).
17. Ihara, M. *et al.* Light-driven hydrogen production by a hybrid complex of a [NiFe]-hydrogenase and the cyanobacterial photosystem I. *Photochem. Photobiol.* **82**, 676–682 (2006).
18. Das, R. *et al.* Integration of photosynthetic protein molecular complexes in solid-state electronic devices. *Nano Lett.* **4**, 1079–1083 (2004).
19. Jordan, P. *et al.* Three-dimensional structure of cyanobacterial photosystem I at 2.5 Å resolution. *Nature* **411**, 909–917 (2001).
20. Evans, P. K. & Krogmann, D. W. 3 c-type cytochromes from the red alga *Porphyridium cruentum*. *Archives Biochem. Biophys.* **227**, 494–510 (1983).
21. Ho, K. K., Ulrich, E. L., Krogmann, D. W. & Gomezlojero, C. Isolation of photosynthetic catalysts from cyanobacteria. *Biochim. Biophys. Acta* **545**, 236–248 (1979).
22. Nakamura, Y. *et al.* Complete genome structure of the thermophilic cyanobacterium *T. elongatus* BP-1. *DNA Res.* **9**, 123–130 (2002).
23. Cho, Y. S., Wang, Q. J., Krogmann, D. & Whitmarsh, J. Extinction coefficients and midpoint potentials of cytochrome c(6) from the cyanobacteria *Arthrospira maxima*, *Microcystis aeruginosa* and *Synechocystis* 6803. *Biochim. Biophys. Acta-Bioenergetics* **1413**, 92–97 (1999).
24. Anta, J. A., Casanueva, F. & Oskam, G. A numerical model for charge transport and recombination in dye-sensitized solar cells. *J. Phys. Chem. B* **110**, 5372–5378 (2006).
25. Duran, R. V., Hervás, M., De la Rosa, M. A. & Navarro, J. A. *In vivo* photosystem I reduction in thermophilic and mesophilic cyanobacteria: the thermal resistance of the process is limited by factors other than the unfolding of the partners. *Biochem. Biophys. Res. Commun.* **334**, 170–175 (2005).
26. Du, H. B., Fairbridge, C., Yang, H. & Ring, Z. The chemistry of selective ring-opening catalysts. *Appl. Catalysis A—General* **294**, 1–21 (2005).
27. Hegedus, L. & Mathe, T. Hydrogenation of pyrrole derivatives—Part V. Poisoning effect of nitrogen on precious metal on carbon catalysts. *Appl. Catalysis A—General* **226**, 319–322 (2002).
28. Irandoust, S. & Edvardsson, J. Poisoning of nickel-based catalysts in fat hydrogenation. *J. Am. Oil Chemists Soc.* **70**, 1149–1156 (1993).
29. Grimme, R. A., Lubner, C. E., Bryant, D. A. & Golbeck, J. H. Photosystem I/molecular wire/metal nanoparticle bioconjugates for the photocatalytic production of H₂. *J. Am. Chem. Soc.* **130**, 6308–6309 (2008).

Acknowledgements

This work was supported by a National Science Foundation (NSF) Nanoscience Interdisciplinary Research Team (NIRT) award to B.D.B. (DBI-0403781) and an NSF Sustainable Science Grant (CBET 0828615) award to P.D.F. and B.D.B. A SARIF Award and Science Alliance Award provided additional support to P.D.F. and B.D.B. The authors would like to acknowledge the technical help of J. Dunlap, A. Godman, C. Pacquet, P. Mahbubani and S. Wright, and also thank G. Alexandre, B. Evans, E. Greenbaum, D. Harrell, L. Johnson and B. Mullin for their input.

Author contributions

I.J.I. performed all the hydrogen evolution experiments, provided data analysis and assisted in manuscript preparation. M.V. grew and maintained *T. elongatus*, isolated and characterized PSI, assisted in cytochrome-*c* isolation, conducted thermostability measurements, composed all the figures, provided data analysis and manuscript preparation. N.M. cloned and developed the over-expression system for cytochrome-*c* and provided cytochrome-*c* for hydrogen evolution experiments. H.O.N. supervised hydrogen evolution experiments, helped coordinate the hydrogen experimentation, and participated in data analysis and manuscript preparation. P.F. coordinated hydrogen evolution experiments, supported I.J.I. and N.M., and participated in data analysis and manuscript preparation. B.D.B. provided overall coordination of the project, supervised the microbiology, molecular biology and biochemistry, provided support for M.V. and N.M., and participated in data analysis and manuscript preparation as corresponding author.

Additional information

The authors declare no competing financial interests. Supplementary information accompanies this paper at www.nature.com/naturenanotechnology. Reprints and permission information is available online at <http://npg.nature.com/reprintsandpermissions/>. Correspondence and requests for materials should be addressed to B.D.B.